Distinct guard cell specific remodeling of chromatin accessibility during abscisic acid and CO_2 dependent stomatal regulation

Authors
Charles A. Seller[1*] and Julian I. Schroeder[1*]

Affiliations
1. School of Biological Sciences
Cell and Developmental Biology Department
University of California San Diego,
La Jolla, CA 92093-0116
*Corresponding authors. Email: cseller@ucsd.edu; jischroeder@ucsd.edu

Classification: Plant Biology

Keywords: Guard cells, stomata, chromatin, plant hormones, abscisic acid, transcription factors, carbon dioxide

Abstract

In plants, epidermal guard cells integrate and respond to numerous environmental signals to control stomatal pore apertures thereby regulating gas exchange. Chromatin structure controls transcription factor access to the genome, but whether large-scale chromatin remodeling occurs in guard cells during stomatal movements, and in response to the hormone abscisic acid (ABA) in general, remain unknown. Here we isolate guard cell nuclei from *Arabidopsis thaliana* plants to examine whether the physiological signals, ABA and CO_2, regulate guard cell chromatin during stomatal movements. Our cell type specific analyses uncover patterns of chromatin accessibility specific to guard cells and define novel cis-regulatory sequences supporting guard cell specific gene expression. We find that ABA triggers extensive and dynamic chromatin remodeling in guard cells, roots, and mesophyll cells with clear patterns of cell-type specificity. DNA motif analyses uncover binding sites for distinct transcription factors enriched in ABA-induced and ABA-repressed chromatin. We identify the ABF/AREB bZIP-type transcription factors that are required for ABA-triggered chromatin opening in guard cells and implicate the inhibition of a set of bHLH-type transcription factors in controlling ABA-repressed chromatin. Moreover, we demonstrate that ABA and CO_2 induce distinct programs of chromatin remodeling. We provide insight into the control of guard cell chromatin dynamics and propose that ABA-induced chromatin remodeling primes the genome for abiotic stress resistance.

Significance statement

Specialized leaf cells called guard cells integrate environmental cues to optimally control the size of microscopic stomatal pores. The hormone abscisic acid (ABA), a key regulator of plant drought responses, and changes in atmospheric CO_2 concentration are signals that control stomatal aperture size, but whether these signals also regulate genome packaging into chromatin is unknown. Using guard cell specific chromatin profiling we uncovered regulatory DNA sequences driving specific gene expression in this cell-type. We also discovered that ABA triggers extensive and persistent changes to chromatin structure in guard cells. Unexpectedly, exposure of plants to elevated atmospheric CO_2 had only minimal impact on chromatin dynamics. Furthermore, we identified the specific transcription factors that regulate ABA-induced chromatin dynamics in guard cells.

INTRODUCTION

Organisms evolved mechanisms that connect the activity of their genome to the conditions in their environment. Developmental and environmental signals can impact the genome by regulating transcription factor (TF) binding to cognate DNA sequences known as cis-regulatory elements (CRE) (1). In eukaryotes, this regulation occurs in the context of chromatin where nucleosomes can impede transcription factor binding to target sequences (2, 3). Consequently, the remodeling of chromatin structure to allow access of transcription factors to target DNA is thought to be a key step in gene regulation. Plant hormones are key signaling molecules controlling numerous aspects of plant life that coordinate genome activity with environmental conditions (4, 5). Recent studies have provided insight into how chromatin structure changes during plant development (6–12) and in response to environmental and hormonal stimuli (13–15).

Here we focus on the abscisic acid (ABA) signal transduction pathway to explore the connection between hormone signaling and chromatin structure in plants. ABA is a major plant stress hormone that accumulates in cells and tissues experiencing abiotic stress, especially those linked to plant water-status (16–18). ABA signals through a well understood core module consisting of PYR/PYL/RCAR ABA receptor proteins, PP2C protein phosphatases, and SnRK2 protein kinases (19–21). Upon ABA binding, PYR/PYL/RCAR receptor proteins inactivate PP2C phosphatases resulting in the derepression of SnRK2 kinases. ABA-activated SnRK2 kinases then phosphorylate and thereby directly regulate downstream proteins including numerous transcription factors (22–28). Consequently, ABA triggers the differential expression of thousands of genes in the *Arabidopsis thaliana* genome (4, 29–31). However, it remains unclear, especially at the genome scale, whether ABA signaling reshapes chromatin structure, and how ABA-regulated TFs might function in the context of chromatin.

78 One well known action of ABA is to trigger the closure of the stomatal aperture (17). Stomata
79 are small pores on the surface of the leaf that mediate gas exchange and are formed by a pair
80 of specialized epidermal cells known as guard cells. Guard cells perceive and respond to
81 multiple environmental and hormonal cues in order to optimally regulate the size of the stomatal
82 pore (32–34). For instance, some signals such as elevated atmospheric carbon dioxide (CO_2),
83 ABA, and the immune elicitor Flg22 trigger stomatal closure, while reduced CO_2, light, and heat
84 trigger stomatal opening. Because of their exquisite environmental reactivity, guard cells are an
85 excellent model cell system to investigate how different physiological signals regulate chromatin
86 structure in a cell-type specific manner. Although the recent application of single-cell RNA-seq
87 to *Arabidopsis* has expanded our understanding of gene regulation, these studies often focus on
88 plate-grown seedlings (35, 36) and/or resulted in datasets with limited representation of guard
89 cells (37, 38). To apply epigenomic techniques to the question of how guard cells respond to
90 different stimuli new protocols are needed that can isolate large numbers of pure guard cells
91 from soil grown plants, a more relevant setting for physiological studies.
92
93 In this paper, we describe the development of an approach to purify guard cell nuclei and by
94 deploying this method, uncover how guard cell chromatin structure changes in response to
95 different stimuli that drive stomatal movements. We profiled the chromatin and transcriptional
96 reprogramming in response to ABA in three different developmental contexts – roots, mesophyll
97 cells, and guard cells. We map thousands of loci that gain or lose chromatin accessibility in
98 response to ABA and link these regions to co-regulated transcripts, uncovering a critical role for
99 chromatin dynamics in controlling ABA-dependent transcription. Furthermore, we show that
100 genome-wide and persistent changes to chromatin structure accompany ABA-induced stomatal
101 closure and that four related bZIP transcription factors known as ABRE Binding Factors (ABFs)
102 are required for initiating the majority of ABA-induced chromatin opening. In contrast, we
103 implicate a family of related bHLH-type TFs known as ABA-Kinase Substrates (AKSs) in the

104 maintenance of open chromatin upstream of ABA-repressed genes. Finally, we show that in
105 guard cells, changes to atmospheric CO_2-concentration trigger distinct and more limited
106 chromatin remodeling and gene regulatory programs from those mediated by abscisic acid.
107
108 **RESULTS**
109
110 **ABA induces rapid and genome-wide chromatin remodeling in roots**
111 As an initial test of the relationship between ABA and chromatin we focused on *Arabidopsis*
112 *thaliana* seedlings. To measure changes to chromatin structure we combined fluorescence
113 activated nuclei sorting (FANS) with the Assay for Transposase-Accessible Chromatin with
114 sequencing (ATAC-seq), a quantitative measurement of chromatin accessibility across the
115 genome (39, 40). 50,000 nuclei per sample were isolated using FANS (Fig. S1A). We called
116 25,753 ATAC-seq peaks across all whole seedling and seedling root libraries (Datasets S1 and
117 S2). Genomic regions coinciding with these peaks are known as Accessible Chromatin Regions
118 (ACRs) and predominantly aligned with upstream regulatory regions in the genome (Fig. S1B-
119 E). In contrast, ATAC-seq reads derived from purified genomic DNA did not cluster into defined
120 peaks (Fig. S1B,C). We next treated whole seedlings with ABA and profiled chromatin
121 accessibility after 4 hours. Differential analysis revealed hundreds of regions that significantly
122 gain and lose accessibility in response to ABA (Fig. 1A, Dataset S3).
123
124 To capture the dynamics of ABA-induced chromatin remodeling we focused on roots which can
125 rapidly take up ABA from their surroundings (41, 42). Using FANS, we isolated root nuclei at
126 three different timepoints following ABA treatment (after 45, 120, and 240 minutes) and
127 performed ATAC-seq. Differential analysis revealed that ABA triggers time-dependent changes
128 in chromatin accessibility in roots (Dataset S3). Heatmaps centered over these ABA regulated
129 ACRs illustrate the progressive impact of ABA on chromatin structure, with more regions of the

130 genome changing in ATAC-signal over time (Fig. 1B,C). We observed significant changes to
131 chromatin after only 45 minutes of ABA treatment, with 163 ACRs located in upstream
132 regulatory regions gaining accessibility and 64 losing accessibility (Fig. 1C,E). After 4 hours,
133 ABA had activated 1293 ACRs and repressed 1119 ACRs (Dataset S3). Interestingly, we found
134 that ABA-regulated ACRs tend to be located further away from transcription start sites (> 1kb)
135 than static regions (Fig. 1D). ABA-induced ACRs were associated with downstream genes
136 enriched for gene ontology (GO) terms such as “response to water deprivation”, “response to
137 osmotic stress”, and “response to abscisic acid” (Dataset S6).
138
139 To explore the role of specific transcription factors in orchestrating these changes we performed
140 DNA motif analysis using a set of motifs empirically generated by the in vitro DNA binding assay
141 DAP-seq (43). We found that motifs recognized by ABF/AREB transcription factors such as
142 ABF1/2/3/4 and ABI5 were highly enriched in ABA-induced ACRs (Fig. 1F, example ABF1, p =
143 1e-63, Dataset S7). In contrast, we found that ABA-repressed ACRs showed enrichment for
144 motifs recognized by the related bHLH type transcription factors AKS1, AKS3, and bHLH80
145 (Fig. 1F, example AKS3, p = 1e-32, Dataset S7). Notably, both ABF1/2/3/4 and AKS1/2/3
146 proteins are direct targets of ABA-regulated SnRK2 kinases (22, 24). Previous research has
147 shown a role for ABA-dependent inhibition of bHLH-type AKS transcription factors in the
148 transcriptional repression of the guard cell K^+ channel *KAT1* (24, 44). Interestingly, our findings
149 suggest a larger role for the AKS clade of closely related bHLH proteins in the regulation of
150 ABA-repressed genes. We conclude that ABA can trigger rapid and genome-wide chromatin
151 remodeling in root tissue.
152
153 **Revealing guard cell specific patterns of chromatin accessibility**
154 Encouraged by our findings in whole seedlings and roots we next decided to investigate the
155 effect of ABA on chromatin in mature guard cells. We first developed a FACS-based strategy to

156 purify guard cell nuclei from soil-grown plants. Nuclei were labeled by expressing the histone
157 H2B fused to GFP under the control of the guard cell *pGC1* promoter (45). We first confirmed
158 the guard cell specificity of the H2B-GFP fusion in our transgenic lines using fluorescence
159 microscopy (Fig. 2A) and confirmed that ABA treatment did not alter the guard cell specific
160 expression (Fig. S2A). We first isolated nuclei from leaf epidermal samples harvested from
161 *GC1:H2B-GFP* plants. DAPI stained nuclei preparations were then analyzed using FACS (Fig
162 S2B). We could define a clearly separated GFP-positive population among all detected nuclei
163 (Fig. 2B, Fig. S2C). In contrast to many other cell types in the *Arabidopsis* leaf, guard cells are
164 diploid, and GFP-positive nuclei from *pGC1:H2B-GFP* expressing plants had a 2n DNA content
165 while GFP-negative nuclei were distributed among higher ploidy levels (Fig. 2C). Approximately
166 5% of GFP-positive particles (41 out of 5037 total from a single FACS run) had DAPI content
167 greater than 2N, however we sorted only 2N nuclei for downstream applications. This method
168 allowed us to obtain ~30,000 guard cell nuclei with an estimated purity of 98% (Fig. S2D) from
169 the leaves of 40-50 plants. To assay guard cell chromatin structure, nuclei isolated using this
170 method were used to generate ATAC-seq libraries. The resulting libraries were of high quality
171 with clear concentration of peaks in annotated upstream regulatory regions (Fig. S2E),
172 enrichment of open chromatin fragments (< 100 bp) immediately upstream of transcription start
173 sites (Fig. S2F), strong correlation between biological replicates (Fig. S2G), and high FRiP
174 (fraction of reads in peaks) scores (Dataset S1).
175
176 In parallel, we generated ATAC-seq samples from root nuclei and from FANS-isolated
177 mesophyll nuclei labeled by expression of H2B-GFP from the promoter of the mesophyll
178 expressed Rubisco small subunit 2B gene (Fig. S3A-C) (6). For each tissue/cell-type we
179 compared ATAC-seq libraries derived from three biological replicates. We identified 30,985
180 ATAC-seq peaks across all samples (Dataset S2) and called cell-type enriched peaks using
181 pairwise differentially accessibility analysis. Although most ATAC-seq peaks did not differ

182 significantly among cell types, we found 3272 guard cell enriched ACRs, 1472 mesophyll
183 enriched ACRs, and 3364 root enriched ACRs (Dataset S2). Heatmaps centered over these
184 regions highlight characteristics of cell/tissue specificity in the observed patterns of chromatin
185 accessibility (Fig. 2D, Fig. S4A). Importantly, biological replicates derived from the same
186 tissue/cell-type clustered together in principal component analysis (PCA) underscoring the
187 robustness of this approach (Fig. 2E).
188
189 To evaluate the relationship between guard cell enriched chromatin accessibility and gene
190 expression we performed RNA-seq on both whole leaves and guard cell-enriched samples. We
191 found that regions with high chromatin accessibility specifically in guard cells were associated
192 with elevated transcript levels from the adjacent downstream genes, indicating that we are
193 identifying functional cis-regulatory elements (CREs) (Fig. 2F). Although the correlation between
194 overall promoter chromatin accessibility and downstream transcript level was weak in guard
195 cells (Pearson's r = 0.19, Fig. S4B), we found that differentially accessible ACRs showed higher
196 correlation with downstream gene differential expression (Pearson's r = 0.55, Fig. S4C).
197 Examination of individual gene loci like the guard cell expressed gene *KAT1* (46–48) illustrated
198 the connection between increased upstream accessibility and increased transcript levels (Fig.
199 2G and Fig S4D). By contrast, the mesophyll expressed gene *AOC1* had high chromatin
200 accessibility in mesophyll cells, but minimal upstream ATAC-seq signal in guard cells (Fig. 2G).
201 TF binding motif analysis on guard cell enriched ACRs returned de novo motifs with strong
202 similarity to motifs recognized by known stomatal lineage transcriptional regulators such as the
203 bHLH proteins SPCH, MUTE, and FAMA as well as EDT1 and DOF-type TFs (49–53) (Fig. 2H
204 and Dataset S7). In contrast, we find that WRKY-type TF binding motifs are enriched in regions
205 that are significantly less accessible in guard cells compared to roots and mesophyll cells (Table
206 S7). However, these motifs are recognized by large transcription factor families containing many
207 transcription factors that are not specific to guard cells, for instance SPCH and MUTE are active

208 only early during stomatal lineage development (49, 50). By connecting guard cell specific
209 ACRs with downstream guard cell enriched transcripts we were able to define a set of 827
210 putative regulatory elements preferentially active in guard cells (Table S4). To further confirm
211 that our approach identified functional cis-regulatory regions, we generated transcriptional
212 reporter constructs expressing nuclear localized GFP under the control of the guard cell specific
213 ACRs upstream of the malate-transporter encoding gene *ALMT6* (54) and the wax biosynthesis
214 enzyme-encoding gene *AAE9* (55). Both reporter constructs produced guard cell specific GFP
215 signal in transgenic *Arabidopsis* leaves (Fig. 2I). In summary, we have developed a robust
216 protocol for isolating pure populations of guard cell nuclei allowing us to discover cis-regulatory
217 regions that are active in mature guard cells.
218
219 **ABA induces persistent chromatin remodeling in guard cells during stomatal closure**
220 We next asked whether epigenomic reprogramming occurs during ABA-induced stomatal
221 closure. Soil grown 6-week-old plants were sprayed with 50 uM ABA or control solution. After 3
222 hours, we confirmed a stomatal response by infrared photography (Fig. 3A). To determine if our
223 ABA treatment led to significant transcriptional changes we performed RNA-sequencing on both
224 whole leaf samples (Fig. S5A) and guard cell enriched samples (Fig. 3B). We observed that
225 ABA triggered the differential expression of thousands of transcripts in both whole leaves and
226 guard cells (2142 upregulated and 1574 downregulated in guard cells). As expected, ABA-
227 induced genes are enriched for the pathways “response to water deprivation” (p_value = 1.7e-
228 22), “response to abscisic acid” (pvalue = 4.47e-18), and “response to salt stress (Fig. S5D).
229 Although most of the transcriptional changes induced by ABA were shared between guard cells
230 and whole leaves, we found that 22.7% (488) of ABA-induced transcripts and 42.7% (673) of
231 ABA-repressed transcripts were specific to guard cells (Fig. S5C, Dataset S5). For instance,
232 ABA-regulated expression of the major facilitator protein-encoding gene *AT2G37900* and the
233 gene *AAE9* was only evident in guard cells (Fig. S5E).

234

235 To evaluate if ABA changed chromatin accessibility and whether these changes are sustained
236 over time following a single treatment, we isolated guard cell nuclei at 4 hours and 24 hours
237 after spraying (Fig. 3A). We generated ATAC-seq libraries from three biological replicates per
238 time point. PCA analysis showed that samples clustered together according to treatment (Fig.
239 S6A). Differential chromatin accessibility analysis found that ABA extensively reshapes
240 chromatin structure in guard cells with 2323 ACRs gaining accessibility and 1657 ACRs losing
241 accessibility across the treatment time course (Fig. 3C, Fig. S7A and B, and Dataset S3). We
242 next analyzed the temporal characteristics of this response by comparing the ATAC-seq
243 datasets from the 4-hour and 24-hour timepoints. Our results allowed us to define three
244 categories of ABA-regulated ACRs – early, sustained, and late (Fig. 3D). Strikingly, we found
245 that 1093 of the 2079 (52.6%) ACRs opened by ABA at 4 hours remained open after 24 hours.
246 Of the 975 ACRs closed by ABA at 4 hours 594 (61%) remained closed at 24 hours.
247 Additionally, we found 230 ACRs gained and 682 ACRs lost accessibility only 24 hours after
248 ABA treatment (Fig. 3D). Interestingly, we found differences in downstream gene GO term
249 enrichment between early and late ACRs. For example, the terms “response to light” and
250 “defense response” were strongly enriched in ABA-repressed ACRs only at 24 hours after ABA
251 treatment (Table S6).

252

253 Consistent with our observations in seedling roots (Fig. 1D), we found that ABA-regulated
254 ATAC-seq peaks in guard cells reside further away from transcription start sites (TSS) than non-
255 regulated peaks (> 1kb), indicating that distal regulation may be a characteristic of ABA-
256 controlled CREs (Fig. S6B). ABA-induced ACRs in guard cells are clearly associated with
257 downstream genes that are upregulated transcriptionally by ABA, while ABA-repressed ACRs
258 are associated with genes downregulated by ABA (Fig. 3E). Indeed, ABA-induced changes in
259 chromatin accessibility were correlated with ABA-induced differential expression of downstream

genes (r = 52, Fig. S6C). Examination of individual genes like the ABA-upregulated *MYB121* and the ABA-downregulated *MYB60* (56) illustrate the connection between upstream chromatin accessibility and transcript levels (Fig. 3F). Interestingly, we found that ABA modifies chromatin accessibility upstream of many known regulators of stomatal conductance including *KAT1*, *NCED3*, and *HT1* (57) as well as many other genes with no known stomatal functions (Fig. S6D-K, Table S3).

We next performed TF binding motif analysis on early, sustained, and late ABA-regulated ACRs using a set of DAP-seq derived motifs (43) restricted to those TFs with guard cell expression in our RNA-seq datasets. Both early and sustained ABA-induced ACRs had strong enrichment for motifs recognized by ABRE- binding TFs including ABI5, ABF1,2, and 3 (Fig. 3G). Interestingly, we found that the motifs recognized by CBF2, CBF3, and MYB61 (58–60) were preferentially enriched in early ABA-induced ACRs. ABA-repressed ACRs showed strong enrichment for motifs recognized by a clade of related bHLH-type TFs (Fig. S6L) including AKS1, AKS3, and bHLH80 in both sustained and late categories (Fig. 3H). In contrast, MYB96 motifs were enriched only in late appearing ABA-repressed ACRs (Fig. 3H). Collectively, our results demonstrate that ABA can induce persistent changes to chromatin in guard cells and expose the temporal regulation of different TFs during this response.

By analyzing published genome-wide DAP-seq datasets (39, *56*) we found strong ABF2 DAP-seq signal coincident with ABA-induced ACRs in guard cells (Fig. 3C). DAP-seq signals for ABF1, ABF3, and ABF4 were also enriched over regions that gain accessibility in response to ABA, although to a lesser extent than ABF2 (Fig. S6M). In contrast, ABA-repressed ACRs contained AKS1 DAP-seq binding sites (Fig. 3C). Additionally, unbiased de novo motif discovery (62) returned motifs similar to ABF1 and AKS3 binding sites as the most enriched in ABA-activated and ABA-repressed ACRs, respectively (p = 1e-119 and p = 1e-57). Metaplots of

286 ATAC-seq signal centered over peaks containing these motifs further supported our observation
287 that ABA elevates chromatin accessibility at ABF binding sites and represses chromatin
288 accessibility at AKS binding sites (Fig. S6N). Interestingly, ABA closed chromatin upstream of
289 *AKS3* and decreased *AKS3* transcript levels in guard cells (Fig. 3I). We also observed that
290 GFP-AKS3 signal decreased in ABA-treated guard cells when expressed from its native
291 promoter (Fig. 3J).
292
293 Furthermore, by comparing ABA-induced ACRs from guard cells, mesophyll cells (Fig. S3E-G),
294 and root cells (Fig. 1) we uncovered significant tissue/cell-type specificity in this response (Fig.
295 3K, Fig S7C-L). Interesting, we found that ABA had a much larger impact on chromatin
296 accessibility in guard cells than in the other cell types with more ABA regulated regions (2079
297 ACRs compared with 1293 in roots and 926 in mesophyll) and larger fold changes in
298 accessibility (Dataset S3). In conclusion, we show that ABA drives large scale changes to
299 chromatin structure in guard cells and implicate major roles for the activation of ABFs and
300 inhibition of AKSs in this response.
301
302 **ABF transcription factors are required for ABA-induced chromatin opening in guard cells**
303 The mechanisms that cause ABA-specific chromatin opening are unknown. Given the strong
304 enrichment of ABF binding motifs in ABA-activated ACRs, and their coincidence with ABF *in*
305 *vitro* binding sites, we wondered if these TFs might be required for reshaping chromatin during
306 ABA-induced stomatal closure. To test this, we used the *abf1/2/3/4* (*abfx4*) quadruple mutant
307 which lacks four related ABF proteins that are prominent during vegetative growth (25, 26). We
308 first performed RNA-seq following ABA treatment on leaves from 6-week-old *abf1/2/3/4* (*abfx4*)
309 mutant plants (Fig. S8A). Of the 2257 transcripts that are upregulated by ABA in wild type
310 leaves, 1897 (~84%) depend on ABF1/2/3/4 (Fig. S8B). Interestingly, although ABA increased
311 *ABF1/2/3/4* transcript levels in guard cells we did not find that ABA altered chromatin

312 accessibility in the upstream regions near the corresponding genes (Fig. S8C). We conclude
313 that ABF1/2/3/4 are required for the bulk of ABA-induced gene expression in mature leaf tissue.
314 Plants lacking *ABF1/2/3/4* (*abfx4*) are highly sensitive to drought stress and lose water faster
315 than wild type plants in detached leaf assays (26). Consistent with this, we observed that *abfx4*
316 mutant plants exhibited higher steady-state stomatal conductances than *Col-0* control plants
317 (Fig. S8D).
318
319 Under non-stressed conditions, guard cells have a higher ABA concentration than other leaf cell
320 types (42, 63). Recent studies have provided evidence for basal ABA signaling in guard cells
321 and defined important roles for basal ABA in stomatal function (64, 65). By generating guard cell
322 FANS lines in an *abfx4* mutant background (Fig. S9A) we were able to assess the impact of the
323 loss of ABF1/2/3/4 on guard cell chromatin in non-stressed plants. In the absence of ABA
324 treatment, we observed minimal differences in genome-wide patterns of chromatin accessibility
325 between *WT* and *abfx4* guard cells (Fig S9B, C and Dataset S3) suggesting that basal ABA
326 signaling in guard cells may regulate mainly post-transcriptional stomatal closing mechanisms
327 but does not significantly regulate chromatin structure.
328
329 Next, we asked if the ABF1/2/3/4 are required for the ability of ABA to reshape chromatin
330 structure. Strikingly, loss of *abf1/2/3/4* strongly impaired ABA-induced chromatin opening in
331 guard cells but had less impact on ABA-triggered chromatin closing (Fig. 4A, Dataset S7). Of
332 the 2079 ABA-induced ACRs, 1539 (~74%) required ABF1/2/3/4 for gained accessibility (Fig.
333 4B). ABF-dependent ABA-induced ACRs were strongly enriched for ABREs (example ABF1, p
334 = 1e-86), while ABF-independent ABA-induced ACRs were most strongly enriched for CBF1/2/3
335 motifs (example CBF1, p = 1e-16) (Dataset S7). Examination of individual loci like the ABA-
336 activated genes *DTX37* and *HSFA6B* revealed a close connection between abf-dependent
337 increases in upstream chromatin accessibility and abf-dependent transcription (Fig. 4C).

338

339 We next performed TF motif analysis on ABA-regulated accessible chromatin regions in both
340 *WT* and *abfx4* mutant guard cells. As expected, *abfx4* mutants were depleted for ABRE motif
341 enrichment in ABA-induced ACRs but notably retained enrichment for AKS1, AKS3, and
342 bHLH80 motifs in ABA-repressed ACRs (Fig. 4D, Dataset S7). Additionally, although most TF
343 binding sites lost enrichment in ABA-induced ACRs in the absence of ABF1/2/3/4, we found that
344 enrichment for motifs bound by CBF1/2/3 was preserved. TF binding motifs are often
345 information poor and the presence of a motif at a genomic location does not always lead to TF
346 action. Analysis of published ABF1/2/3/4 binding assays conducted on naked genomic DNA
347 (61) uncovered 11334 binding sites, but only 1315 resided within ABA-induced ACRs in guard
348 cells (Fig. 4E). However, ABA-induced chromatin opening at these ACRs containing ABF-
349 binding sites was strongly impaired in *abfx4* mutant guard cells (Fig. 4F). We reasoned that
350 chromatin structure may determine which *in vitro* ABF binding sites are functional. To test this
351 idea, we examined if ABF DAP-seq peaks found within ABA-induced ACRs could predict ABA-
352 activated transcription. Using our guard cell RNA-seq data, we found that ABF binding sites that
353 reside within regions of ABA regulated open chromatin were more strongly associated with
354 downstream ABA-induced genes than were an equal number of random ABF-binding sites (Fig.
355 4G).

356

357 To examine the temporal characteristics of ABF-dependent chromatin remodeling we focused
358 on roots where ABA can reshape chromatin by 45 mins (Fig. 1C). We performed ATAC-seq on
359 isolated *abfx4* mutant root nuclei over an ABA treatment time course and found that ABA fails to
360 drive progressive chromatin opening in this background (Fig. S10). In *abfx4* mutant roots, 45
361 mins of ABA treatment induced only 2 ACRs compared to 163 in wild type roots. By 2 hours of
362 ABA treatment, only 27 ABA-induced ACRs were present in *abfx4* mutants compared with 601
363 in wild type (Fig. 4H , Fig. S10A, and Dataset S3). However, ABA repressed a similar number of

364 root ACRs in the absence of ABF1/2/3/4 (Fig. 4H and Fig. S10A). Although our data support a
365 general requirement for ABFs in ABA-induced chromatin opening in roots and guard cells, we
366 do find that some guard cell specific ABA-induced ACRs are ABF-dependent (Fig. S10D,E).
367 Collectively, these results demonstrate that the ABF1/2/3/4 transcription factors are required for
368 triggering genome-wide chromatin opening in response to ABA.
369
370 **ABA and changes to atmospheric CO_2 concentration induce distinct chromatin**
371 **remodeling programs in guard cells**
372 Because we observed that ABA has extensive effects on chromatin accessibility in guard cells,
373 we wondered whether chromatin structure may respond to other stimuli that drive stomatal
374 movements. Here we focus on changes to atmospheric CO_2 concentration. Exposure of plants
375 to low CO_2 stimulates stomatal opening while high CO_2 drives stomatal closure (Fig 5A). The
376 exact role of ABA signaling during CO_2 induced stomatal responses is unclear and is a matter of
377 some debate (64–66). Recent studies suggest that although high-CO_2 induced stomatal closure
378 requires basal ABA signaling it does not involve further SnRK2 kinase activation (64, 65).
379 Comparing how these signals impact genome activity could provide new insight into whether
380 and how the mechanisms underlying guard cell responses to ABA and CO_2 may differ.
381
382 To generate low and high CO_2 guard cell ATAC-seq libraries we exposed 6-week-old plants to
383 either 100 ppm CO_2 or 1000 ppm CO_2 for 4 hrs, two treatments that induce robust stomatal
384 responses (Fig 5B). Surprisingly, in contrast to the extensive effect of ABA on chromatin
385 accessibility in guard cells (Fig. 5C), we observed smaller changes in response to low CO_2 (Fig.
386 5D), and minimal changes following treatment with high CO_2 (Fig. 5E). Following exposure of
387 plants to 100 ppm CO_2, 329 ACRs gained accessibility and 487 ACRs lost accessibility while
388 treatment with 1000 ppm CO_2 induced only 11 ACRs and repressed 79 ACRs (Dataset S3).
389 Heatmaps of ATAC-seq signal at ABA and Low CO_2-regulated regions highlighted the specificity

390 of these responses (Fig. 5F, Fig. S7A,B). PCA results comparing our guard cell ATAC-seq
391 datasets from different conditions further support these findings and revealed little difference
392 between control and high CO_2 treatments (Fig. 5G). Examination of individual loci highlights the
393 specificity of these responses, for instance chromatin opening upstream of *ERF113* only
394 occurred in response to ABA while the upstream region of the PP2C-encoding *AT2G25070*
395 gains accessibility only in response to low CO_2 (Fig. S11B-E).
396
397 Analysis of the set relationships among ABA, low CO_2, and high CO_2 regulated ACRs revealed
398 little overlap suggesting that these stimuli control distinct cis-regulatory elements in the genome
399 (Fig. S11A). We did find overlap between ABA-induced and low CO_2-repressed ACRs and
400 between ABA-repressed and low CO_2-induced ACRs. ABA-repressed regions had elevated
401 average ATAC-seq signal in guard cells isolated from plants exposed to 100 ppm [CO_2] (Fig.
402 5F). For instance, ABA-repressed chromatin accessibility upstream of *ALMT6* while low-CO_2
403 treatment enhanced accessibility (Fig. S11D). Interestingly, ABA repressed chromatin
404 accessibility upstream of *HT1*, *BLUS1*, and *CBC2* (67), all key positive regulators of low CO_2-
405 and blue light-induced stomatal opening, while high CO_2 had no effect (Fig. 5H). These data
406 indicate that chromatin remodeling represents an important cross talk point for these stimuli,
407 ensuring robust stomatal closing or opening, depending on the physiological conditions. DNA
408 binding motif analysis further emphasized the distinct regulatory impacts of changes in CO_2
409 concentration and ABA on the genome (Table S7). In contrast with ABA-induced ACRs, we did
410 not find enrichment of ABF binding motifs in low or high CO_2 regulated chromatin (Fig. 5I).
411 Instead, low CO_2 gained ACRs were enriched for motifs recognized by C2C2dof-type TFs which
412 were oppositely enriched only in ABA-repressed ACRs. Collectively, our data demonstrate how
413 different signals that control stomatal movement deploy distinct gene regulatory programs in
414 guard cells.
415

416

417 **DISCUSSION**

418 Abscisic acid triggers changes in gene expression, but whether this transcriptional response
419 depends on chromatin remodeling remained unknown (5). Here, we reveal massive ABA-
420 induced chromatin remodeling pointing to an orchestrated reprogramming of the *Arabidopsis*
421 epigenome by specific sets of transcription factors. We identify regulatory regions of the
422 genome specifically active in guard cells and uncover how the accessibility of these sequences
423 is modified by signals that control stomatal aperture size.

424

425 Guard cell regulation of stomatal aperture size is essential for plant survival under drought
426 stress. Such regulation requires that the guard cells forming the stomatal pore integrate
427 numerous physiological and environmental cues. In this study, we profiled genome-wide
428 chromatin accessibility in tens of thousands of guard cells isolated from soil-grown plants
429 exposed to different stimuli that trigger stomatal movements. Our results lead us to propose that
430 guard cell ABA signaling controls the balance between two opposing chromatin states. Under
431 unstressed conditions, AKS proteins maintain open chromatin at upstream regulatory regions of
432 ABA-repressed genes while ABA-activated genes are kept silent by closed chromatin. Under
433 abiotic stress such as drought, ABA levels rise in guard cells thereby activating SnRK2 kinases
434 which subsequently inhibit AKSs and activate ABFs. This leads to chromatin opening upstream
435 of abiotic stress-activated genes and the loss of chromatin accessibility upstream of stress-
436 repressed genes.

437

438 We uncovered patterns of chromatin accessibility specific to guard cells (Fig. 2D) and identified
439 cis-regulatory regions supporting guard cell specific gene expression (Fig. 2F-I and Dataset S4).
440 We found that ABA induces extensive and cell-type specific chromatin remodeling and that
441 guard cells possess a more extensive response than mesophyll and root cells (Fig. 3K and Fig.

442 S7C-L). Importantly, we find that these ABA-induced chromatin remodeling events correlate with
443 ABA-regulated gene expression (Fig. 3E and S6C). By performing TF-binding motif enrichment
444 and analyzing published DAP-seq data, we hypothesized that the bZIP transcription factors
445 ABF1/2/3/4 may function in ABA-induced chromatin remodeling in guard cells (Fig. 3C,G and
446 Fig. S6M). Interestingly, we find that among *in vitro* ABF binding sites, those occurring within
447 ABA-opened chromatin are most strongly associated with ABA-induced transcription (Fig. 4G),
448 indicating that regulated chromatin accessibility may determine which genomic ABF binding
449 sites are functional. Our experiments in *abf1/2/3/4* quadruple mutant guard cells demonstrate
450 that these four transcription factors are essential for the majority of ABA-triggered chromatin
451 opening (Fig. 4). Furthermore, experiments in root nuclei show that in *abf1/2/3/4* quadruple
452 mutants, even early ABA-induced chromatin remodeling events are strongly impaired (Fig. 4H
453 and Fig. S10), suggesting that ABFs initiate chromatin opening. How ABFs accomplish
454 chromatin opening remains to be determined, but existing literature could be interpreted to
455 support two possible and not necessarily mutually exclusive explanations. (1) Although
456 nucleosomes can restrict TF binding to DNA, some TFs, known as pioneer factors (68, 69),
457 possess the ability to bind their target sequences even within inaccessible chromatin regions. At
458 present, only a handful of pioneer factors have been documented in plants (70). While our data
459 are consistent with ABFs acting as pioneer factors, future biochemical experiments
460 reconstituting ABF binding to nucleosomal DNA are needed to investigate this model. (2) ABFs
461 may recruit chromatin modifying proteins to target sequences which could increase chromatin
462 accessibility. Interestingly, several such molecules including the SWI/SNF ATPase BRM (71,
463 72) and the histone deacetylase HDA9 (73) interact with known ABA signaling components.
464 Furthermore, ABF-binding proteins known as AFPs, which negatively regulate ABA signaling,
465 have been shown to physically interact with histone and chromatin modifying factors (74).
466

467 Although our data support a general requirement for ABF proteins in both roots and guard cells,
468 we also observe that ABA alters chromatin accessibility in a cell-type specific manner. At
469 present we do not understand how ABFs might contribute to cell-type specific regulation of
470 chromatin. Beyond ABF1/2/3/4, our analyses implicated additional TFs in ABA-dependent
471 genome reprogramming (Fig. 3F and 3G), which is consistent with prior research showing that
472 ABA regulates the binding of multiple transcription factors (75). We observed that ~26% of ABA-
473 gained ACRs (540 ACRs) still open in *abfx4* mutant guard cells in response to ABA (Fig. 4B).
474 These ABF-independent regions retained enrichment for CBF1/2/3 binding motifs, suggesting
475 that CBF transcription factors display ABF-independent binding (Fig. 4D). Finally, although ABA-
476 induced chromatin opening is severely impaired in *abf1/2/3/4* quadruple mutant guard cells, we
477 cannot exclude the possibility that other ABRE-binding TFs, in particular ABI5 (76, 77),
478 participate in this process as well.
479
480 Notably, our data suggest that the related bHLH transcription factors AKS1/2/3 play a larger role
481 in the regulation of ABA-repressed genes than was previously thought. Prior research had
482 shown that SnRK2 kinase-dependent inhibition of AKS1/2 was required for the ABA-dependent
483 transcriptional repression of the K+ ion channel gene *KAT1* in guard cells (24). Surprisingly, we
484 found that AKS1 bound many regions in the genome that lose chromatin accessibility in guard
485 cells following ABA treatment (Fig. 3C). Additionally, motifs recognized by AKS1/3 and the
486 related protein bHLH80 were enriched in ABA-repressed ACRs in guard cells (Fig. 3H), as well
487 as in root and mesophyll cells (Fig. 1F, Fig. S3G, Table S7). This observation was further
488 supported by de novo motif analysis (Fig S6N). AKS1 and AKS2 are inhibited by direct ABA-
489 dependent SnRK2 phosphorylation, but their expression was not controlled by ABA signaling
490 (44). We found that in guard cells, ABA represses *AKS3* expression implying that ABA-
491 dependent inhibition of AKS proteins occurs through both transcriptional and phosphorylation-
492 dependent mechanisms (Fig. 3I and J).

493

494 Elevation in the CO_2 concentration in leaves triggers rapid stomatal closing (34). The extent to
495 which elevated atmospheric CO_2 signals through the ABA signal transduction pathway is
496 currently under debate. Different research groups using the same mutants have come to
497 different conclusions regarding direct CO_2 signaling via the early ABA receptor/SnRK2 kinase
498 pathway during CO_2-induced stomatal closure. Our results exposed major differences in how
499 guard cells interpret these stimuli. In contrast to the extensive and persistent changes to
500 chromatin structure induced by ABA (Fig. 3), exposure to elevated CO_2 had minimal impact on
501 genome-wide chromatin accessibility in guard cells (Fig. 5). While ABA controlled chromatin
502 accessibility at 3018 ACRs in the genome, we found that only 90 ACRs were regulated by
503 elevated CO_2 (Fig 5C-E). Additionally, the strong enrichments of ABF binding motifs in gained
504 ACRs and AKS binding motifs in lost ACRs, evident following ABA treatment, are absent during
505 the response to elevated CO_2 (Fig. 5I). The disparity between these two signals at the level of
506 chromatin mirrors the disparity between characteristics of their respective physiological
507 responses. Unlike ABA- and drought-triggered stomatal closure, elevated CO_2-induced stomatal
508 closure is rapidly reversed upon return to ambient CO_2 (64). Such rapid changes in the
509 intercellular CO_2 concentration in leaves occur for example with alternating light intensities (e.g.
510 passing cloud cover) and require rapid reversals of stomatal CO_2 responses. Furthermore, we
511 found that exposure to low CO_2 triggers a distinct program of chromatin remodeling in guard
512 cells (Fig. 5F-I).

513

514 Finally, our results may open new avenues for investigation into two poorly understood features
515 of stomatal biology. Studies in multiple plant species have documented a phenomenon referred
516 to as stomatal “memory” (78, 79). Following drought stress and re-watering, plants typically
517 exhibit delayed and/or slow re-opening of stomata despite rapid recovery of plant water status.
518 Furthermore, guard cells display transcriptional memory where repetitive dehydration stress

519 leads to altered transcript levels in subsequent stress events (80–82). We found that ABA
520 triggered changes to chromatin accessibility in guard cells that can persist for up to 24 hours,
521 which could prime the genome for subsequent abiotic stress exposure (Fig. 3). These shifts
522 occurred at thousands of locations in the genome including upstream of many genes known to
523 regulate stomatal movements as well as many genes with potential functions in stomatal
524 physiology that could be the basis for future studies (Fig. S6 and Dataset S3). Moreover, our
525 findings support crosstalk between ABA and low CO_2 signaling at the chromatin remodeling
526 level. For example, we uncovered that ABA, but not high CO_2, triggered chromatin closing
527 upstream of genes encoding key CO_2-sensing and signaling proteins that promote low CO_2-
528 induced stomatal opening, including *HT1*, *BLUS1*, and *CBC2* (Fig. 5H). This response may
529 contribute to the long-term stomatal closing triggered by drought and ABA by inhibiting
530 mechanisms for low CO_2-induced stomatal opening. ABA-triggered chromatin dynamics may
531 provide a basis for long-term reprogramming of the guard cell genome for abiotic stress survival.
532 We envision that these sustained changes to chromatin structure may store the experience of
533 drought stress and contribute to long-term adjustments of stomatal function.
534

535 **METHODS**

536 **Plant material and growth conditions**

537 The Columbia-0 (Col-0) accession of *Arabidopsis thaliana* was used as the wild-type
538 background. Experiments on seedlings were conducted using plants germinated and grown on
539 1/2 Murashige and Skoog (MS) media (pH 5.7-8) solidified with 1% Phyto-agar. Experiments on
540 mature plants were conducted using plants grown in soil (Sunshine Mix #1) filled plastic pots
541 incubated in a growth chamber (Conviron) under a 12hr-12hr light-dark cycle, a light intensity of
542 100 μmol m^{-2} s^{-1}, a temperature of 22 C, ambient [CO_2], and a relative humidity of 65%. To
543 minimize the impact of environmental variation all experiments were performed on plants grown
544 in two identical growth chambers equipped with [CO_2] control.

545

546 ABA treatments in plate-based experiments were performed using a mesh (100 µm polyester)
547 transfer method. Seeds were germinated on ½ MS agar plates overlaid with sterilized polyester
548 mesh (100 µm). ABA treatments were initiated by transferring 8-day-old seedlings in mass to
549 plates containing 50 µM ABA (Sigma cis/trans-abscisic acid) or to plates containing vehicle
550 control (Ethanol). ABA treatments on soil grown plants were performed by spraying plants with
551 50 µM ABA diluted with 0.01% Silwet (in water) or with vehicle control. To assess treatment
552 responses, leaf temperature was measured using an infrared thermal imaging camera (T650sc;
553 FLIR).

554

555 **Plasmid DNA and plant transformation**

556 Constructs for cell-type specific nuclear sorting were prepared using multi-site gateway
557 technology (Invitrogen). The ORF encoding the histone H2B (*AT5G22880*) was cloned in a
558 pDONR221 entry vector. The cell type specific promotors RBCp and GC1p, from the Rubisco
559 small subunit 2B gene (*AT5G38420)* and the *GASA9* (*AT1G22690*) gene respectively, were
560 cloned from the *Arabidopsis* genome into the gateway entry vector pDONR-p4p1r. Final plant
561 transformation constructs were generated by performing multisite gateway recombination into
562 the pP7m34GW destination vector. The plasmid for expressing *GFP-AKS3* under the *AKS3*
563 (*AT2G42280*) endogenous promotor was generated using GreenGate cloning (83). The cloned
564 *AKS3* upstream regulatory sequence was defined using guard cell ATAC-seq data.
565 Transcriptional reporter constructs expressing nuclear localized GFP under the guard cell
566 specific ACRs upstream of *AAE9* (*AT1G21540*) and *ALMT6* (*AT2G17470*) were generated
567 using GreenGate cloning. Primer sequences are available in Dataset S8. Constructs were
568 transformed into *A. thaliana* Col-0 plants using floral dipping with *Agrobacterium tumefaciens*
569 strain GV3101.

570

571 **Fluorescence-activated nuclear sorting (FANS)**

572 FANS on seedling/root nuclei and mesophyll nuclei was performed similar to (40) with small
573 modifications. Briefly, whole seedlings, surgically isolated roots, or leaves were chopped
574 vigorously with a clean razor blade in 2-3 ml of ice-cold FANS-lysis buffer (15 mM Tris-HCl
575 pH7.5, 20 mM NaCl, 80 mM KCl, 0.2 mM spermine, 5 mM 2-ME, 0.5 mM spermidine, 0.2%
576 IGEPAL CA-630, Roche mini EDTA-free Protease Inhibitor Cocktail) for 5 minutes in a cold
577 glass petri dish. The subsequent lysate was filtered through a 40 µm filter unit before
578 transferring to a 15 ml tube containing 3 ml of FANS-Sucrose buffer (20 mM Tris-HCl pH 8.0, 2
579 mM $MgCl_2$, 2 mM EDTA, 15 mM 2-ME, 1.7 M sucrose, 0.2% IGEPAL CA-630). Nuclei were
580 pelleted at 2500xG at 4ºC for 25 mins, after which the supernatant was carefully removed. The
581 nuclei pellet was then gently resuspended, using clipped pipette tips, with 600 µl FANS-lysis
582 buffer supplemented with DAPI, and then immediately used for flow cytometry.
583 For experiments on guard cells, the leaves of ~40 six-week-old plants were harvested and
584 blended in 500 ml of ice-cold water for 2x40 secs with 1 min between pulses. The blended
585 sample was poured over a 100 µm mesh to remove mesophyll cells and collect epidermal
586 enriched fragments. The mesh was rinsed with ~200 ml of cold water and gently blotted with
587 paper towels to remove excess liquid. Thin sections of epidermal tissue were then flash-frozen
588 in liquid nitrogen. Epidermal sections were ground to a fine powder with a frozen mortar and
589 pestle. After grinding, powder was transferred to a new mortar with a frozen metal spatula.
590 Immediately 12-15 ml of ice-cold FANS-lysis buffer was added, and the powder was gently
591 resuspended with a clean pestle. The subsequent lysate was filtered through a 40 µm filter unit
592 before transferring to a 15 ml tube containing 6 ml of FANS-Sucrose buffer. Nuclei were then
593 pelleted and prepared for FACS as above.
594
595 Flow cytometry was conducted on a BD FACS Aria II using a 70 µm nozzle with a flow rate < 2
596 and the following photomultiplier parameters: Forward Scatter (FSC) – 250 eV, Side Scatter

597 (SSC) – 220 eV, BV421 (DAPI channel) – 550 eV, FITC (GFP channel) – 340 eV. Sort gates
598 were defined empirically using the FSC and SSC channels to exclude debris and potential
599 doublets. Before sorting GFP labeled nuclei, FACS analysis on unlabeled control samples (Col-
600 0 nuclei) was performed to define background fluorescence signal. When isolating guard cell
601 nuclei, sort gates were established to purify exclusively 2N (diploid) and GFP-positive nuclei. To
602 evaluate the purity of sorted samples, a fraction (~10% of total volume) was re-run under the
603 same sorting program (Fig. S2D). Sorted nuclei were collected in 600 µl of FANS-lysis buffer in
604 a refrigerated tube chamber. After sorting, nuclei were pelleted by centrifugation at 1000xg for
605 10 mins at 4C. Nuclei pellets were gently washed with 1 ml of 10 mM Tris-HCl pH 8.0, 5 mM
606 MgCl2 buffer, before centrifugation again as above. After carefully removing the supernatant,
607 nuclei were used immediately for ATAC-seq.
608
609 Detailed methods descriptions for microscopy and time-resolved stomatal conductance
610 measurements can be found in the SI Appendix, Materials and Methods. Detailed protocols for
611 RNA-seq and ATAC-seq library preparation and description of ATAC-seq, RNA-seq, and DAP-
612 seq data analyses can be found in the SI Appendix, Materials and Methods.
613
614 **Competing interest statement**
615 The authors declare no competing interests.
616
617 **Acknowledgements**
618 Funding for this study was provided by the National Institutes of Health (R01GM060396 to J.I.S
619 and F32GM137544 to C.A.S). CO_2 experiments were supported by National Science
620 Foundation grant MCB-1900567 to J.I.S. This study includes data generated at the UC San
621 Diego IGM Genomics Center utilizing an Illumina NovaSeq 6000 that was purchased with
622 funding from a National Institutes of Health SIG grant (#S10 OD026929). Microscopy was

supported by the UC San Diego Microscopy Core with funding by grant NINDS P30NS047101. We thank Kazuko Yamaguchi-Shinozaki (University of Tokyo) for sharing *abf1/2/3/4* quadruple mutant seeds, and members of the Schroeder lab for helpful discussions throughout the research.

Author contributions: C.A.S. and J.I.S. conceived of the study and designed the methodology. C.A.S. performed all experiments and analyzed the data. C.A.S. and J.I.S. wrote and edited the paper.

Data and materials availability: All materials (plasmids, seed stocks) are available upon request. Raw FASTQ files generated in this study and ATAC-seq peak files in narrowPeak format are available at NCBI's Gene Expression Omnibus under accession GSE243473. All data are available in the main text and supplementary material.

635 **REFERENCES**
636

637 1. R. J. Schmitz, E. Grotewold, M. Stam, Cis-regulatory sequences in plants: Their
638 importance, discovery, and future challenges. *The Plant Cell* **34**, 718–741 (2022).

639 2. W. K. M. Lai, B. F. Pugh, Understanding nucleosome dynamics and their links to gene
640 expression and DNA replication. *Nature Reviews Molecular Cell Biology* **18**, 548–562
641 (2017).

642 3. T. C. Voss, G. L. Hager, Dynamic regulation of transcriptional states by chromatin and
643 transcription factors. *Nature Reviews Genetics* **15**, 69–81 (2014).

644 4. J. L. Nemhauser, F. Hong, J. Chory, Different Plant Hormones Regulate Similar Processes
645 through Largely Nonoverlapping Transcriptional Responses. *Cell* **126**, 467–475 (2006).

646 5. R. Waadt, *et al.*, Plant hormone regulation of abiotic stress responses. *Nat Rev Mol Cell*
647 *Biol* **23**, 680–694 (2022).

648 6. P. Sijacic, M. Bajic, E. C. McKinney, R. B. Meagher, R. B. Deal, Changes in chromatin
649 accessibility between Arabidopsis stem cells and mesophyll cells illuminate cell type-
650 specific transcription factor networks. *The Plant Journal* **94**, 215–231 (2018).

651 7. K. A. Maher, *et al.*, Profiling of Accessible Chromatin Regions across Multiple Plant
652 Species and Cell Types Reveals Common Gene Regulatory Principles and New Control
653 Modules. *The Plant Cell* **30**, 15–36 (2018).

654 8. A. M. Sullivan, *et al.*, Mapping and Dynamics of Regulatory DNA in Maturing Arabidopsis
655 thaliana Siliques. *Frontiers in Plant Science* **10** (2019).

656 9. A. Farmer, S. Thibivilliers, K. H. Ryu, J. Schiefelbein, M. Libault, Single-nucleus RNA and
657 ATAC sequencing reveals the impact of chromatin accessibility on gene expression in
658 Arabidopsis roots at the single-cell level. *Molecular Plant* **14**, 372–383 (2021).

659 10. M. Borg, *et al.*, Epigenetic reprogramming rewires transcription during the alternation of
660 generations in Arabidopsis. *eLife* **10**, e61894 (2021).

661 11. A. P. Marand, Z. Chen, A. Gallavotti, R. J. Schmitz, A cis-regulatory atlas in maize at
662 single-cell resolution. *Cell* **184**, 3041-3055.e21 (2021).

663 12. E.-D. Kim, *et al.*, Dynamic chromatin accessibility deploys heterotypic cis/trans-acting
664 factors driving stomatal cell-fate commitment. *Nat. Plants* **8**, 1453–1466 (2022).

665 13. K. C. Potter, J. Wang, G. E. Schaller, J. J. Kieber, Cytokinin modulates context-dependent
666 chromatin accessibility through the type-B response regulators. *Nat. Plants* **4**, 1102–1111
667 (2018).

668 14. M. A. Reynoso, *et al.*, Evolutionary flexibility in flooding response circuitry in angiosperms.
669 *Science* **365**, 1291–1295 (2019).

670 15. E. S. Karaaslan, N. Faiß, C. Liu, K. W. Berendzen, Isolation of Lineage Specific Nuclei
671 Based on Distinct Endoreduplication Levels and Tissue-Specific Markers to Study
672 Chromatin Accessibility Landscapes. *Plants* **9**, 1478 (2020).

673 16. S. R. Cutler, P. L. Rodriguez, R. R. Finkelstein, S. R. Abrams, Abscisic Acid: Emergence of
674 a Core Signaling Network. *Annual Review of Plant Biology* **61**, 651–679 (2010).

675 17. R. Finkelstein, Abscisic Acid Synthesis and Response. *Arabidopsis Book* **11** (2013).

676 18. J.-K. Zhu, Abiotic Stress Signaling and Responses in Plants. *Cell* **167**, 313–324 (2016).

677 19. Y. Ma, *et al.*, Regulators of PP2C Phosphatase Activity Function as Abscisic Acid Sensors.
678 *Science* **324**, 1064–1068 (2009).

679 20. S.-Y. Park, *et al.*, Abscisic Acid Inhibits Type 2C Protein Phosphatases via the PYR/PYL
680 Family of START Proteins. *Science* **324**, 1068–1071 (2009).

681 21. T. Umezawa, *et al.*, Type 2C protein phosphatases directly regulate abscisic acid-activated
682 protein kinases in Arabidopsis. *Proceedings of the National Academy of Sciences* **106**,
683 17588–17593 (2009).

684 22. H. Fujii, P. E. Verslues, J.-K. Zhu, Identification of Two Protein Kinases Required for
685 Abscisic Acid Regulation of Seed Germination, Root Growth, and Gene Expression in
686 Arabidopsis. *The Plant Cell* **19**, 485–494 (2007).

687 23. K. E. Hubbard, N. Nishimura, K. Hitomi, E. D. Getzoff, J. I. Schroeder, Early abscisic acid
688 signal transduction mechanisms: newly discovered components and newly emerging
689 questions. *Genes Dev.* **24**, 1695–1708 (2010).

690 24. Y. Takahashi, *et al.*, bHLH Transcription Factors That Facilitate K+ Uptake During
691 Stomatal Opening Are Repressed by Abscisic Acid Through Phosphorylation. *Science*
692 *Signaling* **6**, ra48–ra48 (2013).

693 25. T. Yoshida, *et al.*, AREB1, AREB2, and ABF3 are master transcription factors that
694 cooperatively regulate ABRE-dependent ABA signaling involved in drought stress
695 tolerance and require ABA for full activation. *The Plant Journal* **61**, 672–685 (2010).

696 26. T. Yoshida, *et al.*, Four Arabidopsis AREB/ABF transcription factors function predominantly
697 in gene expression downstream of SnRK2 kinases in abscisic acid signalling in response
698 to osmotic stress. *Plant, Cell & Environment* **38**, 35–49 (2015).

699 27. P. Wang, *et al.*, Quantitative phosphoproteomics identifies SnRK2 protein kinase
700 substrates and reveals the effectors of abscisic acid action. *Proceedings of the National*
701 *Academy of Sciences* **110**, 11205–11210 (2013).

702 28. T. Umezawa, *et al.*, Genetics and Phosphoproteomics Reveal a Protein Phosphorylation
703 Network in the Abscisic Acid Signaling Pathway in Arabidopsis thaliana. *Sci. Signal.* **6**,
704 rs8–rs8 (2013).

705 29. N. Leonhardt, *et al.*, Microarray Expression Analyses of Arabidopsis Guard Cells and
706 Isolation of a Recessive Abscisic Acid Hypersensitive Protein Phosphatase 2C Mutant.
707 *The Plant Cell* **16**, 596–615 (2004).

708 30. H. Goda, *et al.*, The AtGenExpress hormone and chemical treatment data set:
709 experimental design, data evaluation, model data analysis and data access. *The Plant*
710 *Journal* **55**, 526–542 (2008).

711 31. R.-S. Wang, *et al.*, Common and unique elements of the ABA-regulated transcriptome of
712 Arabidopsis guard cells. *BMC Genomics* **12**, 216 (2011).

713 32. A. M. Hetherington, F. I. Woodward, The role of stomata in sensing and driving
714 environmental change. *Nature* **424**, 901–908 (2003).

715 33. S. M. Assmann, T. Jegla, Guard cell sensory systems: recent insights on stomatal
716 responses to light, abscisic acid, and CO2. *Current Opinion in Plant Biology* **33**, 157–167
717 (2016).

718 34. G. Dubeaux, *et al.*, Deep dive into CO2-dependent molecular mechanisms driving stomatal
719 responses in plants. *Plant Physiology* **187**, 2032–2042 (2021).

720 35. Z. Liu, *et al.*, Global Dynamic Molecular Profiling of Stomatal Lineage Cell Development by
721 Single-Cell RNA Sequencing. *Molecular Plant* **13**, 1178–1193 (2020).

722 36. C. B. Lopez-Anido, *et al.*, Single-cell resolution of lineage trajectories in the Arabidopsis
723 stomatal lineage and developing leaf. *Developmental Cell* **56**, 1043-1055.e4 (2021).

724 37. J.-Y. Kim, *et al.*, Distinct identities of leaf phloem cells revealed by single cell
725 transcriptomics. *The Plant Cell* **33**, 511–530 (2021).

726 38. C. Procko, *et al.*, Leaf cell-specific and single-cell transcriptional profiling reveals a role for
727 the palisade layer in UV light protection. *The Plant Cell* **34**, 3261–3279 (2022).

728 39. J. D. Buenrostro, P. G. Giresi, L. C. Zaba, H. Y. Chang, W. J. Greenleaf, Transposition of
729 native chromatin for fast and sensitive epigenomic profiling of open chromatin, DNA-
730 binding proteins and nucleosome position. *Nature Methods* **10**, 1213–1218 (2013).

731 40. Z. Lu, B. T. Hofmeister, C. Vollmers, R. M. DuBois, R. J. Schmitz, Combining ATAC-seq
732 with nuclei sorting for discovery of cis-regulatory regions in plant genomes. *Nucleic Acids*
733 *Research* **45**, e41 (2017).

734 41. A. M. Jones, *et al.*, Abscisic acid dynamics in roots detected with genetically encoded
735 FRET sensors. *eLife* **3**, e01741 (2014).

736 42. R. Waadt, *et al.*, FRET-based reporters for the direct visualization of abscisic acid
737 concentration changes and distribution in Arabidopsis. *eLife* **3**, e01739 (2014).

738 43. R. C. O'Malley, *et al.*, Cistrome and Epicistrome Features Shape the Regulatory DNA
739 Landscape. *Cell* **165**, 1280–1292 (2016).

740 44. Y. Takahashi, T. Kinoshita, M. Matsumoto, K. Shimazaki, Inhibition of the Arabidopsis
741 bHLH transcription factor by monomerization through abscisic acid-induced
742 phosphorylation. *The Plant Journal* **87**, 559–567 (2016).

743 45. Y. Yang, A. Costa, N. Leonhardt, R. S. Siegel, J. I. Schroeder, Isolation of a strong
744 Arabidopsis guard cell promoter and its potential as a research tool. *Plant Methods* **4**, 6
745 (2008).

746 46. J. A. Anderson, S. S. Huprikar, L. V. Kochian, W. J. Lucas, R. F. Gaber, Functional
747 expression of a probable Arabidopsis thaliana potassium channel in Saccharomyces
748 cerevisiae. *Proceedings of the National Academy of Sciences* **89**, 3736–3740 (1992).

749 47. D. P. Schachtman, J. 1. Schroeder, W. J. Lucas, J. A. Anderson, R. F. Gaber, Expression
750 of an Inward-Rectifying Potassium Channel by the Arabidopsis KAT1 cDNA. *Science* **258**,
751 1654–1658 (1992).

752 48. R. L. Nakamura, *et al.*, Expression of an Arabidopsis Potassium Channel Gene in Guard
753 Cells. *Plant Physiology* **109**, 371–374 (1995).

754 49. O. S. Lau, *et al.*, Direct roles of SPEECHLESS in the specification of stomatal self-
755 renewing cells. *Science* **345**, 1605–1609 (2014).

756 50. S.-K. Han, *et al.*, MUTE Directly Orchestrates Cell-State Switch and the Single Symmetric
757 Division to Create Stomata. *Developmental Cell* **45**, 303-315.e5 (2018).

758 51. K. Ohashi-Ito, D. C. Bergmann, Arabidopsis FAMA Controls the Final
759 Proliferation/Differentiation Switch during Stomatal Development. *The Plant Cell* **18**, 2493–
760 2505 (2006).

761 52. H. Yu, *et al.*, Activated Expression of an Arabidopsis HD-START Protein Confers Drought
762 Tolerance with Improved Root System and Reduced Stomatal Density. *The Plant Cell* **20**,
763 1134–1151 (2008).

764 53. J. Negi, *et al.*, A Dof Transcription Factor, SCAP1, Is Essential for the Development of
765 Functional Stomata in Arabidopsis. *Current Biology* **23**, 479–484 (2013).

766 54. S. Meyer, *et al.*, Malate transport by the vacuolar AtALMT6 channel in guard cells is
767 subject to multiple regulation. *The Plant Journal* **67**, 247–257 (2011).

768 55. S. Li, *et al.*, Arabidopsis ACYL-ACTIVATING ENZYME 9 (AAE9) encoding an isobutyl-CoA
769 synthetase is a key factor connecting branched-chain amino acid catabolism with iso-
770 branched wax biosynthesis. *New Phytologist* **233**, 2458–2470 (2022).

771 56. E. Cominelli, *et al.*, A Guard-Cell-Specific MYB Transcription Factor Regulates Stomatal
772 Movements and Plant Drought Tolerance. *Current Biology* **15**, 1196–1200 (2005).

773 57. M. Hashimoto, *et al.*, Arabidopsis HT1 kinase controls stomatal movements in response to
774 CO2. *Nat Cell Biol* **8**, 391–397 (2006).

775 58. Y.-K. Liang, *et al.*, AtMYB61, an R2R3-MYB Transcription Factor Controlling Stomatal
776 Aperture in Arabidopsis thaliana. *Current Biology* **15**, 1201–1206 (2005).

59. M. B. Prouse, M. M. Campbell, Interactions between the R2R3-MYB Transcription Factor, AtMYB61, and Target DNA Binding Sites. *PLOS ONE* **8**, e65132 (2013).

60. S. J. Gilmour, *et al.*, Low temperature regulation of the Arabidopsis CBF family of AP2 transcriptional activators as an early step in cold-induced COR gene expression. *The Plant Journal* **16**, 433–442 (1998).

61. Y. Sun, *et al.*, Divergence in the ABA gene regulatory network underlies differential growth control. *Nat. Plants*, 1–12 (2022).

62. S. Heinz, *et al.*, Simple Combinations of Lineage-Determining Transcription Factors Prime cis-Regulatory Elements Required for Macrophage and B Cell Identities. *Molecular Cell* **38**, 576–589 (2010).

63. W. Lahr, K. Raschke, Abscisic-acid contents and concentrations in protoplasts from guard cells and mesophyll cells ofVicia faba L. *Planta* **173**, 528–531 (1988).

64. P.-K. Hsu, *et al.*, Abscisic acid-independent stomatal CO2 signal transduction pathway and convergence of CO2 and ABA signaling downstream of OST1 kinase. *Proceedings of the National Academy of Sciences* **115**, E9971–E9980 (2018).

65. L. Zhang, *et al.*, FRET kinase sensor development reveals SnRK2/OST1 activation by ABA but not by MeJA and high CO2 during stomatal closure. *eLife* **9**, e56351 (2020).

66. M. Dittrich, *et al.*, The role of Arabidopsis ABA receptors from the PYR/PYL/RCAR family in stomatal acclimation and closure signal integration. *Nat. Plants* **5**, 1002–1011 (2019).

67. A. Hiyama, *et al.*, Blue light and CO2 signals converge to regulate light-induced stomatal opening. *Nat Commun* **8**, 1284 (2017).

68. M. Iwafuchi-Doi, K. S. Zaret, Pioneer transcription factors in cell reprogramming. *Genes Dev.* **28**, 2679–2692 (2014).

69. A. Balsalobre, J. Drouin, Pioneer factors as master regulators of the epigenome and cell fate. *Nat Rev Mol Cell Biol*, 1–16 (2022).

70. R. Jin, *et al.*, LEAFY is a pioneer transcription factor and licenses cell reprogramming to floral fate. *Nat Commun* **12**, 626 (2021).

71. S.-K. Han, *et al.*, The SWI2/SNF2 Chromatin Remodeling ATPase BRAHMA Represses Abscisic Acid Responses in the Absence of the Stress Stimulus in Arabidopsis. *The Plant Cell* **24**, 4892–4906 (2012).

72. M. Peirats-Llobet, *et al.*, A Direct Link between Abscisic Acid Sensing and the Chromatin-Remodeling ATPase BRAHMA via Core ABA Signaling Pathway Components. *Molecular Plant* **9**, 136–147 (2016).

73. D. Baek, *et al.*, Histone Deacetylase HDA9 With ABI4 Contributes to Abscisic Acid Homeostasis in Drought Stress Response. *Frontiers in Plant Science* **11** (2020).

74. T. J. Lynch, B. J. Erickson, D. R. Miller, R. R. Finkelstein, ABI5-binding proteins (AFPs) alter transcription of ABA-induced genes via a variety of interactions with chromatin modifiers. *Plant Mol Biol* **93**, 403–418 (2017).

75. L. Song, *et al.*, A transcription factor hierarchy defines an environmental stress response network. *Science* **354**, 1550 (2016).

76. R. Finkelstein, S. S. L. Gampala, T. J. Lynch, T. L. Thomas, C. D. Rock, Redundant and Distinct Functions of the ABA Response Loci ABA-INSENSITIVE(ABI)5 and ABRE-BINDING FACTOR (ABF)3. *Plant Mol Biol* **59**, 253–267 (2005).

77. R. R. Finkelstein, T. J. Lynch, The Arabidopsis Abscisic Acid Response Gene ABI5 Encodes a Basic Leucine Zipper Transcription Factor. *The Plant Cell* **12**, 599–609 (2000).

78. E. Fleta-Soriano, M. Pintó-Marijuan, S. Munné-Bosch, Evidence of Drought Stress Memory in the Facultative CAM, Aptenia cordifolia: Possible Role of Phytohormones. *PLOS ONE* **10**, e0135391 (2015).

79. P. A. Auler, F. B. S. Freire, V. F. Lima, D. M. Daloso, On the role of guard cells in sensing environmental signals and memorising stress periods. *Theor. Exp. Plant Physiol.* **34**, 277–299 (2022).

80. Y. Ding, M. Fromm, Z. Avramova, Multiple exposures to drought “train” transcriptional responses in *Arabidopsis*. *Nature Communications* **3**, 740 (2012).

81. L. Virlouvet, M. Fromm, Physiological and transcriptional memory in guard cells during repetitive dehydration stress. *New Phytologist* **205**, 596–607 (2015).

82. A. van Weringh, A. Pasha, E. Esteban, P. J. Gamueda, N. J. Provart, Generation of guard cell RNA-seq transcriptomes during progressive drought and recovery using an adapted INTACT protocol for Arabidopsis thaliana shoot tissue. 2021.04.15.439991 (2021).

83. A. Lampropoulos, *et al.*, GreenGate - A Novel, Versatile, and Efficient Cloning System for Plant Transgenesis. *PLOS ONE* **8**, e83043 (2013).

FIGURES LEGENDS

Figure 1. ABA induces rapid and genome-wide chromatin remodeling in seedlings. A) Volcano plot of differential ATAC-seq analysis showing regions that significantly change in chromatin accessibility in seedlings after 4hrs of ABA treatment. ABA increased accessibility at 666 regions and decreased accessibility at 214 regions (FDR < 0.001 and FC > 1.5, differential peaks colored in red). **B)** Heatmap of root nuclei ATAC-seq signal (RPKM-normalized) centered over ATAC-seq peaks (+/- 1.5 kb) with ABA-regulated chromatin accessibility during the indicated ABA treatment time course. Across all timepoints, ABA increased accessibility at 1293 regions and decreased accessibility at 1119 regions (FDR < 0.001 and FC > 1.5). **C)** Number of ABA-regulated ATAC-seq peaks over time in roots. ABA-induced peaks are colored in blue while ABA-repressed peaks are colored in pink. **D)** Distribution among annotated genomic features of either all ATAC-seq peaks (orange) or ABA-regulated ATAC-seq peaks (grey). **E)** Genome browser snapshots at two representative genes (*MAPKKK18* and *CML25*) showing changes in ATAC-seq signal in upstream regions following ABA treatment. Scale bars indicate 500 bp. **F)** The transcription factor binding motifs with the highest enrichment (by binomial p-value) in ABA-induced and ABA-repressed chromatin regions in roots.

Fig 2. Cell-type specific epigenomics identifies guard cell specific regulatory elements. A) Left panel is a fluorescence micrograph showing guard cell specific expression of H2B-GFP. Right panel shows a 3D reconstruction from confocal imaging of a 5-week-old *GC1p:H2B-GFP* leaf (merged image shows GFP fluorescence in green and chlorophyll fluorescence in magenta). **B)** FACS analysis of nuclei (DAPI positive) from *GC1p:H2b-GFP* plants. A GFP density plot defines two distinct populations separated by GFP intensity. **C)** DAPI density plot shows that GFP positive nuclei (blue population) are primarily diploid, while GFP negative nuclei (pink population) are distributed over multiple ploidies. **D)** Chromatin accessibility heatmaps comparing ATAC-seq signal (RPKM-normalized) in guard cell, mesophyll, or root cell nuclei. ATAC-seq peaks are separated into guard cell enriched (3272 ACRs), mesophyll enriched (1472 ACRs), and root enriched (3364 ACRs) sets defined by differential accessibility (p.adj < 0.001, Fold-Change > 2). **E)** Principal component analysis (PCA) comparing ATAC-seq biological replicates derived from guard cell, mesophyll, or root nuclei. **F)** A peak-centered ATAC-seq metaplot and a gene-body centered RNA-seq metaplot showing average chromatin accessibility at guard cell specific peaks and average transcript levels of nearest downstream genes (ATAC-seq peak within -2.5 kb and +0.5 kb of transcription start site). Guard cell derived signal is shown in black while mesophyll/leaf signal is shown in green. **G)** Genome browser images displaying ATAC-seq and RNA-seq signal for the indicated tracks near the guard cell expressed gene *KAT1* and the mesophyll cell expressed gene *AOC1*. Scale bars indicate 500 bp. **H)** Results of de novo motif analysis using homer are shown along with the best matching known TFs and the enrichment p-values. **I)** Transcriptional reporter lines generated using cloned guard cell specific ACRs upstream of the genes *AAE9* and *ALMT6,* the positions of the cloned sequences are indicated with orange highlighting on the genome browser images (scale bars indicate 500 bp). Confocal micrographs showing GFP fluorescence (left panel) or merged GFP (green) and chlorophyll (magenta) fluorescence (right panel). Scale bar represents 20 µm.

904 **Figure 3. ABA triggers extensive and persistent chromatin remodeling in guard cells.**
905 **A)** Schematic showing the experimental outline. Plants were sprayed with ABA and infrared images
906 were taken using a thermal camera to assess stomatal closure. Guard cell nuclei were purified at
907 4hrs and 24 hrs after treatment and used for ATAC-seq. **B)** Volcano plot of guard cell enriched RNA-
908 seq data showing that ABA upregulates 2142 transcripts and downregulates 1574 transcripts (FDR <
909 0.001, FC > 2.0). Differentially expressed transcripts are colored in red. **C)** Heatmaps and profile
910 plots of ATAC-seq signal (RPKM-normalized) in guard cell nuclei centered (+/- 1.5 kb) over 2323
911 regions with ABA-induced chromatin accessibility and 1657 regions with ABA-repressed chromatin
912 accessibility (FDR < 0.001, FC > 2.0). The adjacent heatmaps show DAP-seq signal for ABF2 (in
913 red) and AKS1 (in black) centered over the same ABA regulated ACRs, data from (39) and (56). **D)**
914 Comparison of ABA-regulated peaks from 4hr and 24hr timepoints separated ACRs into three
915 categories – early only, sustained (both early and late), and late only. The bar graph shows the
916 number of ABA-increased and -decreased regions in each category. **E)** (Top) Metaplots showing
917 average ATAC-seq signal centered over either ABA-induced or ABA-repressed ACRs and (bottom)
918 RNA-seq metaplots showing average transcript level centered over gene bodies downstream of the
919 same ACRs. Signal from ABA-treated plants is shown in orange and signal from control treated
920 plants is shown in black. **F)** Genome browser images showing guard cell ATAC-seq and RNA-seq
921 signal at a representative ABA-induced gene (*MYB121)* and an ABA-repressed gene (*MYB60*).
922 Scale bars indicated 500 bp. **G,H)** Heatmaps showing TF binding motif enrichments (-log(p-value))
923 in ABA-increased **(G)** and ABA-decreased **(H)** ATAC-seq peaks. **I)** Genome browser images
924 showing guard cell ATAC-seq and RNA-seq signal at the *AKS3* gene. Scale bars indicated 500 bp.
925 **J)** Fluorescence micrograph showing expression of *AKS3pr::GFP-AKS3* in guard cells after
926 treatment with control or ABA (4 hr). **K)** Overlap of ABA-induced accessible regions in guard cell
927 nuclei, mesophyll nuclei, and root nuclei.
928
929
930 **Fig 4. ABF transcription factors are required for ABA-induced chromatin opening in**
931 **guard cells. A)** Heatmaps of ATAC-seq signal (RPKM-normalized) in either *WT* or *abfx4*
932 mutant guard cells centered over 2079 regions with ABA-induced accessibility and 975 regions
933 with ABA-repressed accessibility (FDR < 0.001 and FC > 2.0). ACRs are subdivided by
934 requirement for ABF1/2/3/4 **B)** Overlap of ABA-induced ATAC-seq peaks in *WT* guard cells with
935 those in *abfx4* mutant guard cells. **C)** Genome browser snapshots showing ATAC-seq and
936 RNA-seq signal near two ABA-induced genes *DTX37* and *HSFA6B*. Scale bars indicate 1 kb. **D)**
937 Enrichment (-log(p-value)) of the indicated transcription factor binding motifs in ABA regulated
938 ATAC-seq peaks in either *WT* or *abfx4* mutant guard cell nuclei. **E)** Overlap between ABF DAP-
939 seq peaks and ABA-induced accessible chromatin regions (ACRs). **F)** Peak-centered metaplot
940 showing ATAC-seq signal in the indicated samples at ABA-induced ACRs containing ABF DAP-
941 seq binding sites. **G)** 1000 ABF DAP-seq peaks overlapping ABA-induced ATAC-seq peaks or
942 1000 random ABF DAP-seq peaks were assigned to nearest downstream genes (within -2.5 kb
943 and +0.5 kb of TSS). The plot shows the ABA-induced fold changes within these two sets of
944 downstream transcripts. Asterisks (****) indicate that the distributions are significantly different
945 by Welch's t-test (p < 1E-7) and the red bars represent the means of the distributions. **H)** Bar
946 plots representing the number of ABA-activated or ABA-repressed ACRs over time in *Col-0* or
947 *abfx4* mutant roots.
948
949
950 **Fig 5. ABA and changes in CO_2 concentration induce distinct chromatin remodeling**
951 **programs in guard cells. A)** Diagram showing the effects of different stimuli on the stomatal
952 aperture. **B)** Representative IR image showing differences in leaf temperature due to CO_2
953 induced stomatal movement. **C-E)** Volcano plots of differential ATAC-seq results showing **C)**
954 ABA-regulated chromatin accessibility, **D)** low CO_2 regulated chromatin accessibility, and **E)**
955 high CO2 regulated chromatin accessibility. The numbers of differentially accessible peaks

956 (colored in red, FDR < 0.001 and FC > 2.0) in each condition are indicated on each plot. **F)**
957 Heatmaps and profile plots of guard cell ATAC-seq signal centered over either ABA-regulated
958 ACRs (2079 induced and 975 repressed) or low CO_2-regulated ACRs (329 induced and 487
959 repressed). Libraries are derived from plants exposed to the indicated treatments. **G)** Principal
960 component analysis (PCA) shows that ABA, low CO_2, and high CO_2 introduce separate variation
961 to genome-wide chromatin accessibility. **H)** Genome browser images showing ABA-repression
962 of chromatin accessibility upstream of *HT1*, *BLUS1*, and *CBC1* – three positive regulators of low
963 CO_2 induced stomatal opening. Scale bars indicate 1 kb. **I)** Enrichment (-log P_value) of the
964 indicated transcription factor binding motifs in ABA, Low CO_2, or High CO_2 regulated regions.
965 Negative enrichment scores indicate motifs overrepresented in treatment-repressed regions. No
966 significant enrichment for any of these motifs was found in High CO_2 regulated ACRs.
967
968

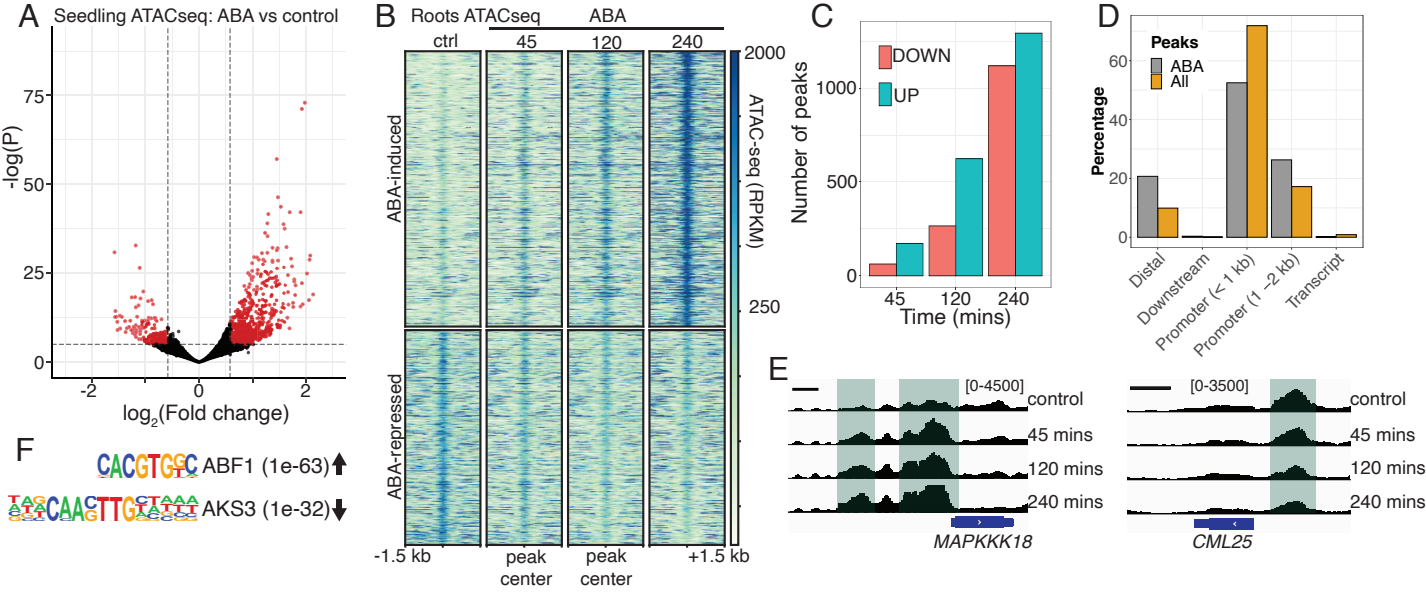
A
Seedling ATACseq: ABA vs control
-log(P)
75
50
25
0
-2
0
2
log2(Fold change)
B
Roots ATACseq
ABA
ctrl
45
120
240
ABA-induced
ABA-repressed
2000
250
ATAC-seq (RPKM)
-1.5 kb
peak center
peak center
+1.5 kb
C
DOWN
UP
Number of peaks
1000
500
0
45
120
240
Time (mins)
D
Peaks
ABA
All
Percentage
60
40
20
0
Distal
Downstream
Promoter (< 1 kb)
Promoter (1 –2 kb)
Transcript
E
[0-4500]
control
45 mins
120 mins
240 mins
MAPKKK18
[0-3500]
control
45 mins
120 mins
240 mins
CML25
F
ABF1 (1e-63)
AKS3 (1e-32)

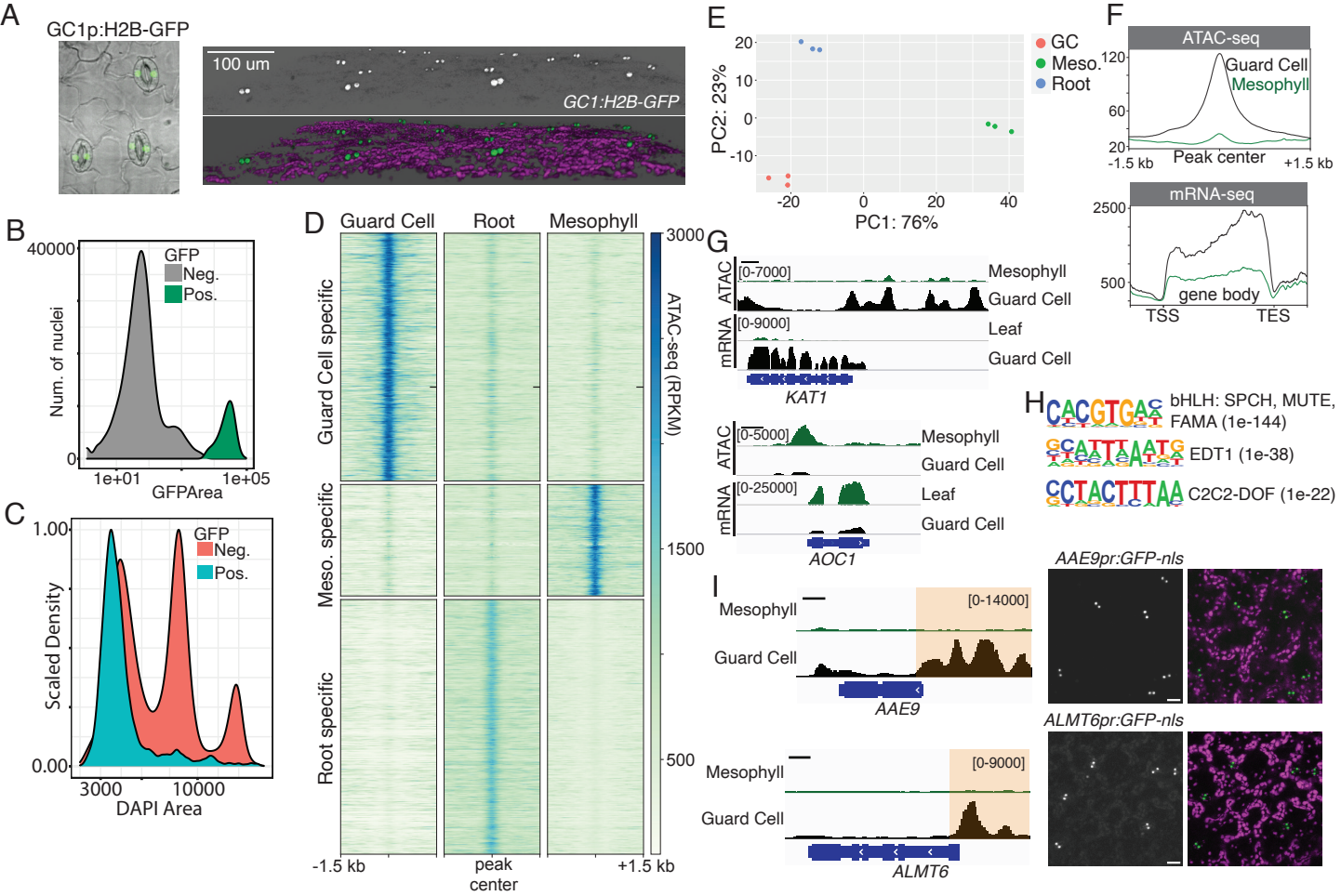
A
GC1p:H2B-GFP
100 um
GC1:H2B-GFP
B
GFP
Neg.
Pos.
Num. of nuclei
40000
0
1e+01
1e+05
GFPArea
C
GFP
Neg.
Pos.
Scaled Density
1.00
0.00
3000
10000
DAPI Area
D
Guard Cell
Root
Mesophyll
Guard Cell specific
Meso. specific
Root specific
ATAC-seq (RPKM)
3000
1500
500
-1.5 kb
peak center
+1.5 kb
E
GC
Meso.
Root
PC2: 23%
PC1: 76%
20
10
0
-10
-20
0
20
40
F
ATAC-seq
Guard Cell
Mesophyll
120
60
20
-1.5 kb
Peak center
+1.5 kb
mRNA-seq
2500
500
gene body
TSS
TES
G
ATAC
[0-7000]
Mesophyll
Guard Cell
mRNA
[0-9000]
Leaf
Guard Cell
KAT1
ATAC
[0-5000]
Mesophyll
Guard Cell
mRNA
[0-25000]
Leaf
Guard Cell
AOC1
H
bHLH: SPCH, MUTE, FAMA (1e-144)
EDT1 (1e-38)
C2C2-DOF (1e-22)
I
Mesophyll
Guard Cell
[0-14000]
AAE9
Mesophyll
Guard Cell
[0-9000]
ALMT6
AAE9pr:GFP-nls
ALMT6pr:GFP-nls

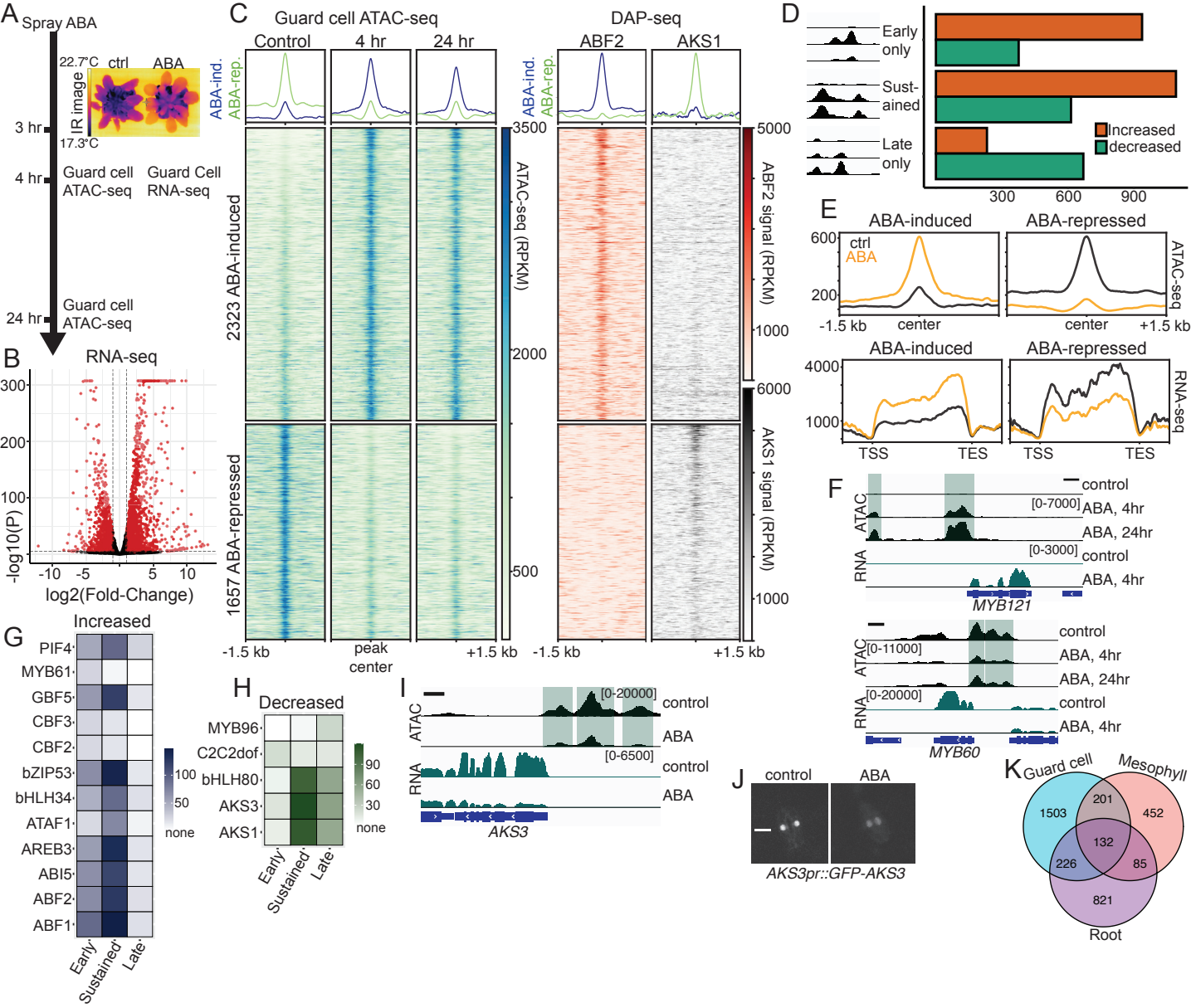
A
Spray ABA
22.7°C
ctrl
ABA
IR image
17.3°C
3 hr
4 hr
Guard cell ATAC-seq
Guard Cell RNA-seq
24 hr
Guard cell ATAC-seq
B
RNA-seq
-log10(P)
log2(Fold-Change)
C
Guard cell ATAC-seq
Control
4 hr
24 hr
DAP-seq
ABF2
AKS1
ABA-ind.
ABA-rep.
2323 ABA-induced
1657 ABA-repressed
ATAC-seq (RPKM)
ABF2 signal (RPKM)
AKS1 signal (RPKM)
-1.5 kb
peak center
+1.5 kb
D
Early only
Sust-ained
Late only
Increased
decreased
E
ABA-induced
ABA-repressed
ctrl
ABA
ATAC-seq
RNA-seq
TSS
TES
F
ATAC
RNA
control
ABA, 4hr
ABA, 24hr
MYB121
MYB60
G
Increased
PIF4
MYB61
GBF5
CBF3
CBF2
bZIP53
bHLH34
ATAF1
AREB3
ABI5
ABF2
ABF1
Early
Sustained
Late
none
H
Decreased
MYB96
C2C2dof
bHLH80
AKS3
AKS1
I
ATAC
RNA
control
ABA
AKS3
J
control
ABA
AKS3pr::GFP-AKS3
K
Guard cell
Mesophyll
Root
1503
201
452
132
226
85
821

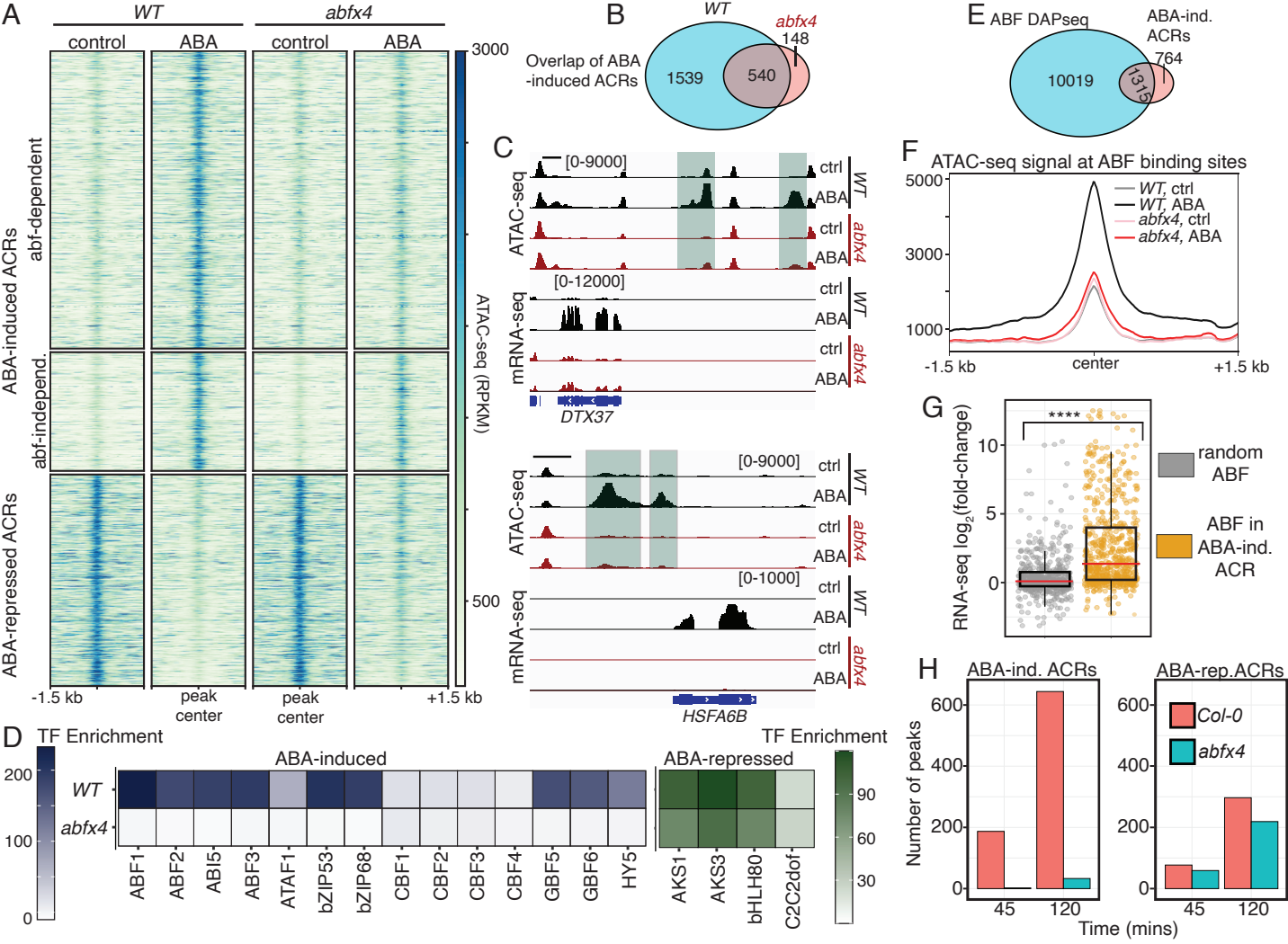
A
WT
abfx4
control
ABA
control
ABA
ABA-induced ACRs
abf-dependent
abf-independ.
ABA-repressed ACRs
3000
ATAC-seq (RPKM)
500
-1.5 kb
peak center
peak center
+1.5 kb
B
WT
abfx4
148
Overlap of ABA -induced ACRs
1539
540
E
ABF DAPseq
ABA-ind. ACRs
764
10019
1315
C
[0-9000]
ATAC-seq
ctrl
ABA
WT
abfx4
[0-12000]
mRNA-seq
DTX37
[0-9000]
[0-1000]
HSFA6B
F
ATAC-seq signal at ABF binding sites
5000
3000
1000
WT, ctrl
WT, ABA
abfx4, ctrl
abfx4, ABA
-1.5 kb
center
+1.5 kb
G
RNA-seq log2(fold-change)
****
10
5
0
random ABF
ABF in ABA-ind. ACR
D
TF Enrichment
200
100
0
ABA-induced
WT
abfx4
ABF1
ABF2
ABI5
ABF3
ATAF1
bZIP53
bZIP68
CBF1
CBF2
CBF3
CBF4
GBF5
GBF6
HY5
ABA-repressed
AKS1
AKS3
bHLH80
C2C2dof
90
60
30
H
ABA-ind. ACRs
ABA-rep.ACRs
Number of peaks
600
400
200
0
Col-0
abfx4
45
120
Time (mins)

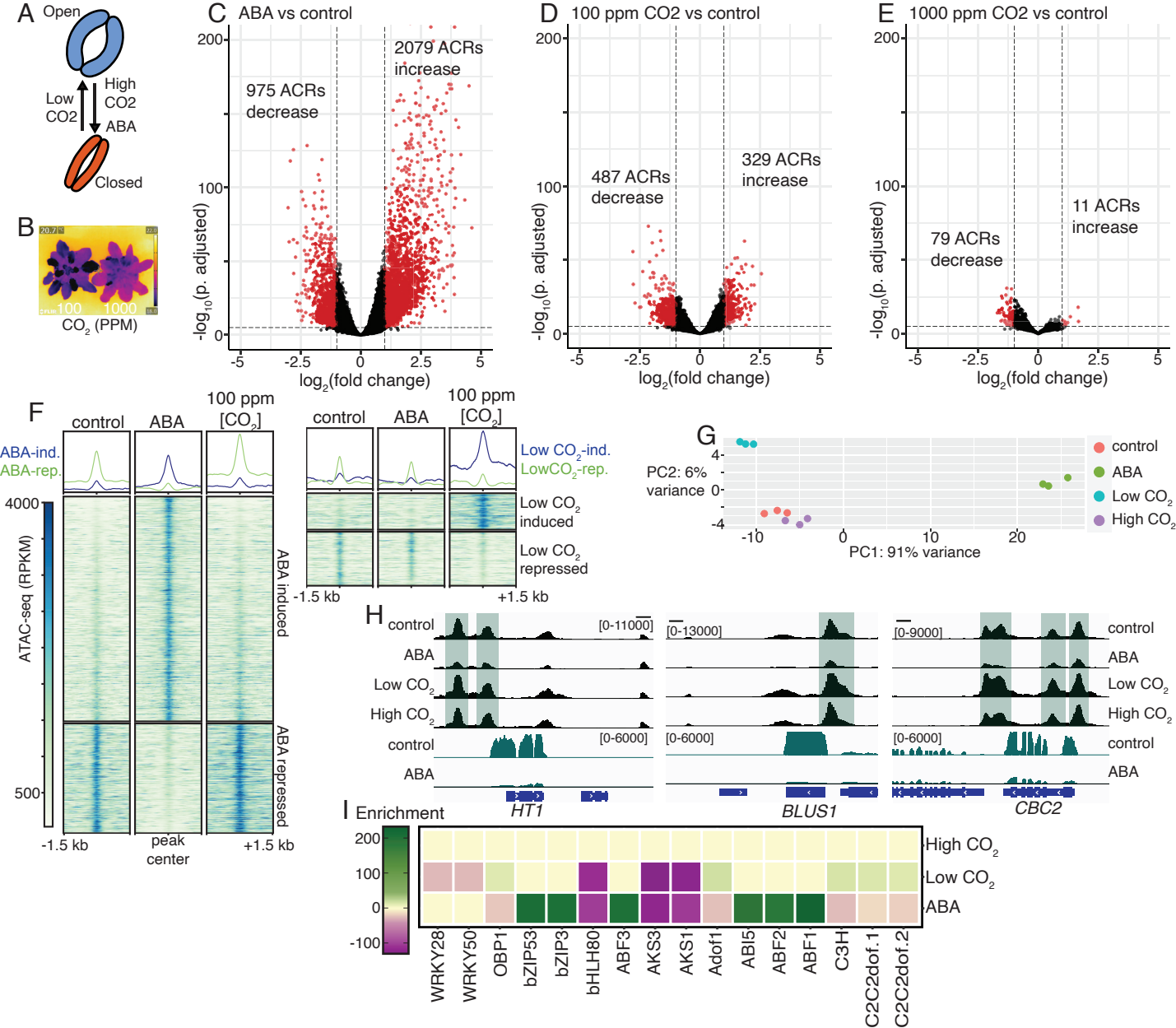
A
Open
Low CO2
High CO2
ABA
Closed
B
100
1000
CO2 (PPM)
C
ABA vs control
975 ACRs decrease
2079 ACRs increase
-log10(p. adjusted)
log2(fold change)
D
100 ppm CO2 vs control
487 ACRs decrease
329 ACRs increase
E
1000 ppm CO2 vs control
79 ACRs decrease
11 ACRs increase
F
control
ABA
100 ppm [CO2]
ABA-ind.
ABA-rep.
ATAC-seq (RPKM)
4000
500
ABA induced
ABA repressed
-1.5 kb
peak center
+1.5 kb
Low CO2-ind.
LowCO2-rep.
Low CO2 induced
Low CO2 repressed
G
PC2: 6% variance
PC1: 91% variance
control
ABA
Low CO2
High CO2
H
[0-11000]
[0-13000]
[0-9000]
[0-6000]
HT1
BLUS1
CBC2
I
Enrichment
High CO2
Low CO2
ABA
WRKY28
WRKY50
OBP1
bZIP53
bZIP3
bHLH80
ABF3
AKS3
AKS1
Adof1
ABI5
ABF2
ABF1
C3H
C2C2dof.1
C2C2dof.2